Ultrasound-mediated Delivery of Paclitaxel for Glioma: A Comparative Study of Distribution, Toxicity, and Efficacy of Albumin-bound Versus Cremophor Formulations

Daniel Y. Zhang[1], Crismita Dmello[1], Li Chen[1], Victor A. Arrieta[1,8], Edgar Gonzalez-Buendia[1], J. Robert Kane[1], Lisa P. Magnusson[1], Aneta Baran[1], C. David James[1], Craig Horbinski[1,2], Alexandre Carpentier[3,4], Carole Desseaux[5], Michael Canney[5], Miguel Muzzio[6], Roger Stupp[1,7], and Adam M. Sonabend[1,7]

ABSTRACT

Purpose: Paclitaxel shows little benefit in the treatment of glioma due to poor penetration across the blood–brain barrier (BBB). Low-intensity pulsed ultrasound (LIPU) with microbubble injection transiently disrupts the BBB allowing for improved drug delivery to the brain. We investigated the distribution, toxicity, and efficacy of LIPU delivery of two different formulations of paclitaxel, albumin-bound paclitaxel (ABX) and paclitaxel dissolved in cremophor (CrEL-PTX), in preclinical glioma models.

Experimental Design: The efficacy and biodistribution of ABX and CrEL-PTX were compared with and without LIPU delivery. Antiglioma activity was evaluated in nude mice bearing intracranial patient-derived glioma xenografts (PDX). Paclitaxel biodistribution was determined in sonicated and nonsonicated nude mice. Sonications were performed using a 1 MHz LIPU device (SonoCloud), and fluorescein was used to confirm and map BBB disruption. Toxicity

of LIPU-delivered paclitaxel was assessed through clinical and histologic examination of treated mice.

Results: Despite similar antiglioma activity *in vitro*, ABX extended survival over CrEL-PTX and untreated control mice with orthotopic PDX. Ultrasound-mediated BBB disruption enhanced paclitaxel brain concentration by 3- to 5-fold for both formulations and further augmented the therapeutic benefit of ABX. Repeated courses of LIPU-delivered CrEL-PTX and CrEL alone were lethal in 42% and 37.5% of mice, respectively, whereas similar delivery of ABX at an equivalent dose was well tolerated.

Conclusions: Ultrasound delivery of paclitaxel across the BBB is a feasible and effective treatment for glioma. ABX is the preferred formulation for further investigation in the clinical setting due to its superior brain penetration and tolerability compared with CrEL-PTX.

Introduction

The current standard of care for patients with glioblastoma (GBM) involves surgical resection followed by adjuvant temozolomide chemoradiotherapy, and most recently the addition of tumor-treating fields (1). Nevertheless, GBM remains an ultimately fatal disease as over 90% of patients die within 5 years. Novel treatment strategies are urgently needed. One cause of the commonly observed resistance to conventional therapies is the inability to achieve adequate concentrations in the brain due to the protective blood–brain barrier (BBB; refs. 2, 3).

[1]Department of Neurological Surgery, Northwestern University Feinberg School of Medicine, Chicago, Illinois. [2]Department of Pathology, Northwestern University Feinberg School of Medicine, Chicago, Illinois. [3]Assistance Publique-Hôpitaux de Paris (AP-HP), Hôpitaux Universitaux La Pitié-Salpêtrière, Service de Neurochirurgie, Paris, France. [4]Sorbonne Université, UPMC Univ Paris 06, Paris, France. [5]CarThera, Institut du Cerveau et de la Moelle épinière (ICM), Paris, France. [6]Life Sciences Group, IIT Research Institute, Chicago, Illinois. [7]Lou and Jean Malnati Brain Tumor Institute, Robert H. Lurie Comprehensive Cancer Center, Northwestern University, Chicago, Illinois. [8]PECEM, Faculty of Medicine, National Autonomous University of Mexico, Mexico City, Mexico.

Note: Supplementary data for this article are available at Clinical Cancer Research Online (http://clincancerres.aacrjournals.org/).

Corresponding Author: Adam M. Sonabend, Northwestern University, 676 N St. Clair Street, Suite 2210, Chicago IL 60611. Phone: 312-695-8143; Fax: 312-695-3294; E-mail: adam.sonabend@nm.org

While it is well established that the BBB is disrupted at the site of the tumor bulk, the BBB remains intact in the infiltrating and nonenhancing part of the tumor that is commonly the origin of subsequent tumor recurrence (4–6). Many methods have been developed and tested to bypass the BBB to improve drug delivery for the treatment of GBM. These methods include convection-enhanced delivery (CED), intracranial injections, or directly implanting drug-containing wafers during surgery (7, 8). Each of these methods have their own associated limitations such as reflux in the case of CED or a limited drug diffusion zone in the case of implanted wafers. These limitations prevent drugs from reaching invasive cancer cells in the brain parenchyma distant from the injection/implantation site (9, 10). Alternatively, broad region disruption of the BBB is achievable via intra-arterial delivery of osmotic agents such as mannitol; however, therapeutic efficacy and feasibility of these methods are also limited due to a minimal half-life of BBB disruption (<10 minutes). Furthermore, mannitol requires the need for arterial catheterization, which limits the repeated treatments commonly used in cancer (11).

Ultrasound (US)-mediated BBB disruption is an emerging new technology that makes use of the physical interactions between ultrasonic waves and systemically administered microbubbles to transiently disrupt the BBB (12). This technique has been used to enhance the delivery of a wide range of chemotherapeutic agents such as doxorubicin, carboplatin, and temozolomide across the BBB into the brain (13–15). Preclinical and clinical studies have demonstrated that ultrasound-mediated BBB disruption is well-tolerated in animal models and humans (16–20).

Paclitaxel (PTX), a microtubule stabilizing drug, was initially identified in preclinical models as a potent agent against GBM. According to the Cancer Cell Line Encyclopedia (CCLE) database (21), paclitaxel exhibits robust antiglioma effects *in vitro* with an average

Translational Relevance

Paclitaxel is approximately 1,400-fold more potent than temozolomide, the current standard chemotherapy for glioma, yet it is not used in the clinic due to its inadequate penetration across the blood–brain barrier (BBB). Here, we demonstrate the ability of low-intensity pulsed ultrasound-based BBB opening to increase paclitaxel concentrations in the brain after systemic administration of paclitaxel. Two different FDA-approved formulations of paclitaxel were compared. The albumin-bound formulation of paclitaxel was better tolerated and had increased brain penetration compared with the cremophor-based formulation. Multiple sessions of ultrasound-delivered albumin-bound paclitaxel increased survival in an orthotopic glioma model compared with nonsonicated controls while ultrasound delivered cremophor–paclitaxel induced central nervous system toxicity. Our preclinical experiments suggest that increased paclitaxel drug delivery by disrupting the BBB is feasible, and an effective antiglioma treatment. Albumin-bound paclitaxel is the preferred formulation for further investigation in the clinical setting.

Figure 1.
ABX displays greater bioavailability than CrEL-PTX and increased antiglioma effect *in vivo*. **A,** Comparison of IC_{50} of glioma cell lines across two common chemotherapeutic drugs: TMZ, temozolomide ($n = 34$), paclitaxel ($n = 12$). **B–D,** Biodistribution of ABX and CrEL-PTX. **B,** Plasma paclitaxel concentration at 45 and 180 minutes (*, $P = 0.0285$; **, $P = 0.0056$). **C,** Ratio of brain to plasma paclitaxel concentration at 45 minutes (ABX $n = 9$, CrEL-PTX $n = 7$, $P = 0.0193$) and 180 minutes (ABX $n = 4$, CrEL-PTX $n = 3$, $P = 0.0349$). **D,** Ratio of heart or liver to plasma PTX concentration at 45 minutes (ABX $n = 9$, CrEL-PTX $n = 7$, $P < 0.0001$). Data plotted, mean $\pm$ SD. **E,** *In vivo* antiglioma effect of ABX: MES83 cells were used to establish orthotopic xenografts and groups of 12 mice were randomized to treatment groups as indicated. Survival for each is plotted in Kaplan–Meier graphs and evaluated through log-rank test. Arrows represent treatment days (*, $P = 0.0423$; **, $P = 0.0041$).

IC_{50} concentration nearly 1,400-fold lower than temozolomide (**Fig. 1A**). Yet, several clinical trials investigating paclitaxel for the treatment of GBM demonstrated minimal response (22–25). Studies later determined that while paclitaxel concentration was detectable in tumor tissue, paclitaxel was undetectable within the surrounding brain parenchyma, elucidating the BBB as a major limitation for paclitaxel efficacy for infiltrative disease in gliomas (26, 27).

There are currently two formulations of paclitaxel that are approved for clinical use in humans: Taxol (Generic) and Abraxane (Celgene). Paclitaxel is a highly lipophilic molecule that is very poorly water-soluble. Taxol is formulated by dissolving paclitaxel in Cremophor EL (CrEL) for intravenous administration. Studies have demonstrated that CrEL, a 50:50 mix of polyethoxylated castor oil and dehydrated ethanol, is toxic to the peripheral nervous system, which poses concerns about the safety of this formulation for use in the central nervous system (CNS; refs. 28, 29).

Abraxane is an albumin-bound paclitaxel formulation (ABX) recently introduced as an alternative to Taxol. ABX can be dissolved in water and does not contain CrEL as a vehicle. ABX was found to have a more favorable toxicity profile, in particular, a lower rate (10%) and shorter duration of peripheral neuropathy compared with Taxol (33%) in a large randomized trial of patients with breast cancer (30, 31).

We hypothesized that paclitaxel is an effective agent against GBM if sufficient tumor and brain concentrations can be achieved. Given the concerns of neurotoxicity for CrEL, and the limited brain penetration of conventional paclitaxel formulations, we compared the safety, pharmacokinetic, and efficacy profiles of CrEL dissolved paclitaxel to that of ABX in the presence and absence of LIPU. Our preclinical investigations provide the foundation for clinical exploration of the albumin-bound formulation of paclitaxel in combination with ultrasound-based BBB disruption for patients with GBM.

Materials and Methods

Study drugs

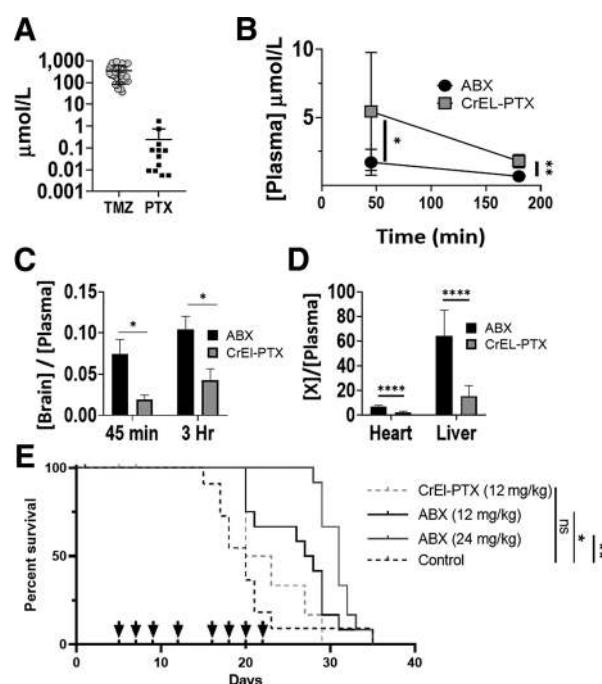Commercially available clinical-grade Abraxane (Celgene) and Taxol (Teva Pharmaceuticals) were purchased from the hospital pharmacy. Drugs were stored at room temperature according to the package insert and prepared the day of experiments.

Animal studies

All animal studies were performed in accordance with Northwestern University's Institutional Animal Care and Usage Committee. Six- to 12-week-old male and female athymic nude (nu/nu) mice purchased from Charles River Laboratories were used in these studies.

Sonication procedure

The sonication procedure was performed using a preclinical LIPU device (SonoCloud Technology) manufactured by CarThera. Mice were anesthetized with ketamine/xylazine (K/X) cocktail (ketamine 100 mg/kg, xylazine 10 mg/kg, i.p.). MB (Lumason, Bracco) were reconstituted according to manufacturer instructions and injected at a dose of 7.5 mL/kg through the retro-orbital route. Shortly after MB administration, mice were quickly (<10 seconds) placed supine upon the ultrasound transducer holder and sonications began. A 1 MHz, 10-mm diameter flat ultrasound transducer was fixed in a holder filled with degassed water and sonications were performed transcranially (Supplementary Fig. S1A). Sonications were performed for 120 seconds using a 25,000 cycle burst at a 1 Hz pulse repetition frequency and

an acoustic pressure of 0.3 MPa as measured in water. After sonications, mice were moved to a clean cage, placed upon a heating pad, and monitored until they recovered from anesthesia.

Fluorescein mapping of BBB disruption and biodistribution studies

Biodistribution studies were performed in healthy nude mice with intact BBB at two time points, 45 and 180 minutes after sonication. Following sonication, mice were injected intravenously with either ABX or CrEL-PTX (12 mg/kg). Forty-five minutes before euthanasia, intravenous NaFl (Sigma-Aldrich) was administered at a dose of 20 mg/kg (Supplementary Fig. S1B). Dosing solutions were prepared by diluting a weighed amount of NaFl powder, ABX powder, or measured volume of Taxol solution with 0.9% saline solution to a final injection volume of 5 mL/kg. Mice were then euthanized with Euthasol (Virbac) solution (150 mg/kg, i.p.) and brains were carefully removed and imaged using Nikon AZ100 Epifluorescent microscope (4×, FITC filter cube, 2-second exposure time). Highly fluorescent areas of the brain were separated from nonfluorescent regions using a clean no. 15 scalpel that was disposed of after every mouse. These samples were placed into separate cryo-vials (Corning) and flash frozen in liquid N_2. Heart, liver, and plasma samples were also collected and immediately flash frozen in liquid N_2. Frozen tissue samples were stored in $-80°C$ freezer for under 45 days before downstream paclitaxel and NaFl concentration analysis.

LC/MS determination of paclitaxel concentration

Paclitaxel was determined in plasma and brain tissue using LC/MS-MS (6500 QTRAP AB Sciex, equipped with a SIL-20AC XR HPLC, Shimadzu Scientific Instruments). For plasma analysis, a 50 μL aliquot of plasma was mixed with 200 μL of acetonitrile containing paclitaxel-d5 (internal standard, 2 ng/mL) in a 96-well deep well plate. After shaking for 5 minutes, the sample was centrifuged at 4,000 rpm for 10 minutes at 4°C. An aliquot of 105 μL of supernatant was transferred to another 96-well deep well plate and diluted with 300 μL of ASTM type 1 water before instrumental analysis. Brain, heart, and liver tissue specimens were finely minced with surgical scalpels and a 30-mg sample was treated with 1 mL of 50/50 acetonitrile/water (v/v), and homogenized in a 1600 MiniG (SPEX SamplePrep) tissue homogenizer for 10 minutes using a stainless steel ball. The resulting tissue homogenates extracts were then processed as above.

Chromatographic separation was achieved with a Kinetex C18, 50 × 2.1 mm, 2.6 μm (Phenomenex) column. The mobile phase was A: 0.1% formic acid in water (v/v) and B: 0.1% formic acid in acetonitrile (v/v). After injection, initial conditions with A at 70% were held for 0.2 minutes, decreased to 30% in 2.8 minutes, and held at 30% for 0.4 minutes before returning to initial conditions within 0.1 minutes and reequilibration for 2.5 minutes before the next sample. The flow rate was 0.4 mL/minute at 25°C. Retention times for paclitaxel and paclitaxel-d5 were both 2.55 minutes with a total run time of 6 minutes. A turbo ion spray interface was used as the ion source operating in positive mode. Acquisition was performed in multiple reaction monitoring mode (MRM) using m/z 854.5 → 286.0, 859.5 → 569.2 ion transitions at low resolution for paclitaxel and paclitaxel-d5, respectively.

NaFl concentration determination

NaFl was determined using a Glomax Multi Detection System (Promega) with a Blue Fluorescence Optical Kit (excitation 490 nm, emission 515–580 nm). For plasma analysis, a 100 μL aliquot of plasma was mixed with 300 μL of 0.1% formic acid in acetonitrile (v/v) in a 2-mL microcentrifuge tube. After shaking for 5 minutes, the sample was centrifuged at 4,000 rpm for 10 minutes at 4°C. An aliquot of 20 μL of supernatant was transferred to a 2-mL microcentrifuge tube and mixed with 380 μL of 10 mmol/L PBS (pH = 8.5). After shaking for 3 minutes, an aliquot of 200 μL sample was transferred into a 96-well black microplate for fluorescence analysis. The sample was protected from light. Brain tissue specimens were homogenized as before and the extracts processed as described for plasma samples.

Toxicity studies

Toxicity of single and multiple courses of ultrasound-delivered paclitaxel was evaluated in nu/nu mice. For single-course toxicity studies, nontumor-bearing healthy mice were used. Following treatment, bodyweight was monitored biweekly for 3 weeks before mice were euthanized and brains were collected for histologic evaluation.

For multiple-course toxicity studies, healthy nontumor-bearing and mice bearing intracranial xenografts were used. Mice receiving ultrasound alone, US-CrEl-PTX (12mg/kg), US-CrEL alone, US-ABX (12 mg/kg), and US-ABX (24 mg/kg) were treated eight times over a period of three weeks (days 1, 3, 5, 8, 12, 14, 16, and 18). CrEL was prepared in house by mixing dehydrated ethanol and Kolliphor EL (Sigma) in a 50:50 ratio. This solution was diluted to 5% in sterile 0.9% saline solution prior to retro-orbital administration at 10 ml/kg. In addition, a separate cohort of mice treated with US-ABX (24 mg/kg) on a different dosing schedule (days 1, 4, 8, 11, 15, 18, 22, and 25) was also evaluated. Bodyweight and survival were monitored throughout treatment period and three weeks after last course of treatment. Mice who died during treatment had their brains collected for histologic evaluation of CNS toxicity. In addition, nontumor-bearing mice were euthanized 21 days after last course of treatment to examine CNS toxicity that did not result in death.

Tissue was prepared for histology evaluation as follows. Following dissection from the cranium, mouse brains were placed into 4% paraformaldehyde solution. After 6–8 days of fixation, brains were transferred to PBS with 0.2% sodium azide (Alfa Aesar) for long-term storage. Brains were dissected halfway between the dorsal and ventral surfaces in the transverse plane or at the midline of the brain in the sagittal plane before being dehydrated in a series of ethanol baths. Following dehydration, brains were embedded in paraffin and sectioned at 4 μm. Sections were stained with Harris Hematoxylin (Surgipath) and Eosin Y Solution (Sigma-Aldrich) and analyzed for histopathology by a neuropathologist blinded to treatment group. Representative images of brain sections were taken at 20× magnification (TissueGnostics) and then stitched together to create whole section images (TissueFaxs).

Intracranial patient-derived xenograft mouse model

Single-cell suspensions (MES83 from Ichiro Nakano, University of Alabama and GBM12 from C. David James, Northwestern University, Evanston, IL) generated from patient tumor samples were serial passaged as heterotrophic flank tumors and short-term explant cultures as described previously prior to intracranial implantation (32). For intracranial implantation, mice were anesthetized with K/X cocktail before a 1-cm incision was made in the midline of the mouse head to expose the skull underneath. A transcranial burr hole was created using sterile hand held drill (Harvard Apparatus) and mouse was mounted on a stereotaxic device (Harvard Apparatus). A total of 2×10^4 MES83 cells or 5×10^4 GBM12 cells in 2.5 μL of sterile PBS were loaded into a 29G Hamilton Syringe and injected slowly over a period of 3 minutes

into the left hemisphere of the mouse brain at 3 mm depth through the transcranial burr hole created 3 mm lateral and 2 mm caudal relative to midline and bregma sutures. Following injection, incision was closed using 9 mm stainless steel wound clips.

Patient-derived xenograft cell viability assay

MES83 and GBM12 cells were cultured as short-term explant cultures in DMEM (Corning) with 10% FBS (GE Health Sciences) and 1% penicillin/streptomycin solution (Corning) prior to being seeded at a density of 4,000 cells per well in a 96-well plate. One day after seeding, cells were checked for attachment and confluence (60%–70%). Media were removed from the wells and 100 μL fresh media with paclitaxel dissolved in DMSO or ABX ranging in concentrations from 0.002 μmol/L to 2 μmol/L was placed into the wells. Seventy-two hours later, cell viability was determined by CellTiter Glo (Promega). PDX identity was confirmed through short tandem repeat analysis. (Supplementary Table S2).

Ultrasound-delivered chemotherapy treatment of patient-derived xenograft mouse model and survival analysis

For MES83 survival studies, five days after tumor implantation, mice ($n = 59$) were distributed equally into five different treatment groups. Mice were anesthetized using K/X cocktail and injected intravenously through the retro-orbital route with either 0.9% sterile saline solution, CrEL-PTX at 12 mg/kg, ABX at 12 mg/kg, ABX at 24 mg/kg, or ABX at 24 mg/kg immediately following sonication treatment. For GBM12 survival studies, five days after tumor implantation, mice ($n = 30$) were distributed equally into three different treatment groups; control (0.9% sterile saline injection), ABX at 24 mg/kg, or ultrasound-delivered ABX at 24 mg/kg.

Primary endpoint of the survival study was defined by the development of neurologic symptoms due to tumor burden. Upon reaching endpoints, mice were sacrificed and their brains were harvested in preserved in 4% PFA. Presence of tumor was confirmed through gross examination of brain sections. Mice that died before such endpoints could be reached, or mice whose brains did not contain tumor were censored from survival analysis. Previous studies performed by our lab as well as others (14, 33) demonstrated that ultrasound alone ($n = 19$) at the parameters used to disrupt the BBB is unable to extend survival, so this group was not included in the current studies.

Statistical analysis

All statistical analysis was performed using Graphpad Software (Prism). Two-tailed Student t test or one-way ANOVA was used to measure statistical differences between two groups or greater than two groups respectively. In vitro dose–response curves were generated by fitting experimental cell viability data to a sigmoidal curve using the inhibitor versus. response–variable slope (four parameters) function. Statistical analysis of animal survival was performed using log-rank test. Pearson correlation coefficient was determined to measure strength of correlation.

Results

ABX exhibits enhanced antiglioma activity compared with CrEL-PTX due to better brain penetration

First, we compared the biodistribution of systemically administered ABX to CrEL-PTX (Fig. 1B–D). Plasma concentration of ABX was significantly lower than CrEL-PTX at both 45 and 180 minutes ($P = 0.0285$ at 45 minutes, $P = 0.0056$ at 180 minutes). Mice receiving ABX showed 4-fold increased mean brain to plasma (B:P)

ratio compared with mice that received CrEL-PTX at 45 minutes after administration ($P = 0.0193$). At 180 minutes, ABX displayed 2-fold greater B:P ratios than CrEL-PTX ($P = 0.0349$). Other systemic organs, such as the heart and liver, showed a similar phenomenon at 45 minutes (Fig. 1D).

We then investigated whether the superior B:P ratio exhibited by ABX was associated with increased antiglioma activity in vivo using a orthotropic PDX model. PDX models are shown to better recapitulate genetic and morphologic characteristics typically found in primary human tumors compared with commercial cell lines (34). We compared the therapeutic effect of CrEL-PTX and ABX at an equivalent dose (12 mg/kg) as well as at a higher dose of ABX (24 mg/kg) against MES83, a primary GBM intracranial PDX. (Fig. 1E; refs. 34, 35). The doses we tested were chosen because they were well tolerated by mice and lead to plasma concentrations similar to those achieved in patients administered 260 mg/m^2 of ABX, which is used for the regimen (every 3 weeks) for metastatic breast cancer (31). Mice treated with CrEL-PTX (12 mg/kg) did not show a significant increase in survival compared with untreated controls; however, the same dose of ABX significantly increased median survival time by 137.5% (27.5 days) compared with untreated controls (20 days, $P = 0.0423$). When the dose of ABX was doubled to 24 mg/kg, median survival increased by 155% (31 days, $P = 0.0041$). CrEL-PTX was not tested at 24 mg/kg, as mice had difficulty tolerating the lower CrEL-PTX/Taxol regimen.

Fluorescein as a visual marker to map ultrasound-based BBB disruption and paclitaxel accumulation in the brain

LIPU was used to disrupt the BBB and fluorescein was investigated as a potential tool to map BBB disruption by ultrasound through the following experiment. Mice were injected intravenously with sodium fluorescein (NaFl) and ABX immediately after sonication/MB injection. Forty-five minutes after NaFl injection, mice brains were harvested and imaged with a fluorescent microscope (Fig. 2A). Fluorescent areas of the brain were then separated from nonfluorescent areas. Brain tissue samples were analyzed for paclitaxel and fluorescein concentrations and compared with samples from nonsonicated control mice. We observed that regions of the brain targeted by the ultrasound device led to accumulation of fluorescein, and fluorescein concentrations were correlated with paclitaxel concentration ($r = 0.8987$, $P < 0.0001$; Fig. 2B). These results confirmed ultrasound-based BBB disruption, and the use of fluorescein as a tool to map regions of the brain where paclitaxel concentrations were elevated following this treatment.

Ultrasound further enhances the brain penetration and efficacy of ABX in intracranial gliomas

To determine the effect of ultrasound-based BBB disruption on paclitaxel concentration within the brain, the fluorescein visualization method described above was used to quantify paclitaxel levels in brain tissue from both sonicated and nonsonicated mice (Fig. 3A).

Fluorescent brain tissue from mice receiving ABX showed a significant 3 to 5-fold increase in paclitaxel B:P ratios compared with nonfluorescent areas and nonsonicated controls at both 45 ($P = 0.0002$) and 180 minutes ($P = 0.0241$; Fig. 3B and C). In contrast, fluorescent brain tissue from mice receiving CrEL-PTX did not show a significant increase in paclitaxel B:P at 45 minutes ($P = 0.219$), but did show a significant increase at 180 minutes ($P = 0.0017$; Fig. 3B and C). Furthermore, absolute concentrations of paclitaxel in fluorescent brain tissue measured in mice receiving ABX
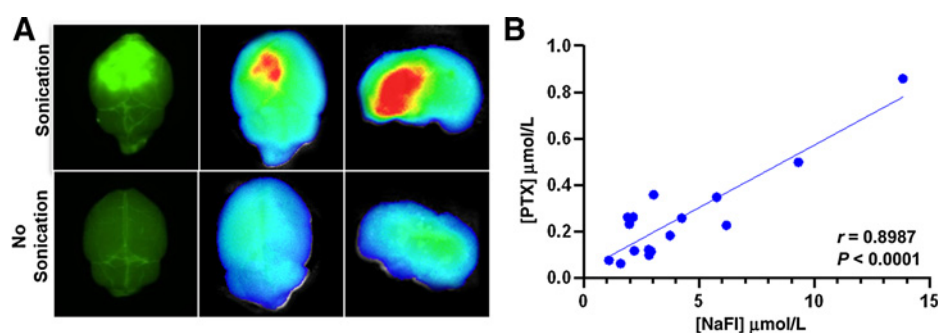
Figure 2.
Sodium fluorescein is a visual marker for ultrasound (US) BBB disruption. **A,** Fluorescent imaging: mice injected intravenously NaFL were treated with ultrasound and compared with nonsonicated controls. Brains were harvested and imaged using Nikon AZ100 microscope at 4× magnification with FITC filter cube (left) and SII Lago *in vivo* Imaging system (ex/em 465/530nm). **B,** NaFl and paclitaxel correlation: 16 brain samples from sonicated and nonsonicated mice were analyzed for NaFl and paclitaxel concentration through LC/MS. Correlation was determined by calculating Pearson coefficient ($r = 0.8987$, $P < 0.0001$).

surpassed IC_{50} values for 10 of 12 glioma cell lines listed in the Sanger/CCLE database (**Fig. 3D**; ref. 21).

Interestingly, the two different formulations of paclitaxel displayed different pharmacokinetic profiles in the context of ultrasound-mediated drug delivery. The absolute brain paclitaxel concentration achieved by ultrasound-delivered ABX remained stable from 45 minutes to 180 minutes ($P = 0.4201$). In contrast, brain paclitaxel concentrations achieved through ultrasound-delivered CrEL-PTX increased nearly 2-fold from 45 minutes to 180 minutes ($P = 0.01$).

We next investigated whether the increase in drug concentrations achieved by ultrasound-based ABX delivery translated into superior efficacy against glioma models *in vivo*. We tested our treatment in two different glioma PDX models, GBM12 and MES83, with differing therapeutic profiles *in vitro* (**Fig. 4A**). In MES83, the PDX line that exhibited more sensitivity to paclitaxel, we observed ultrasound-based delivery of ABX (24 mg/kg) was able to nearly double median survival time (35 days) compared with untreated controls (20 days, $P = 0.0006$). Furthermore, ultrasound-based delivery of ABX further extended median survival time of tumor-bearing mice (35 days) beyond ABX alone (31 days, $P = 0.0036$; **Fig. 4C**).

In mice bearing GBM12 xenografts, the PDX line that exhibited relative resistance to PTX, ABX (24 mg/kg) was also successful in extending survival over control-treated mice (38 vs. 24 days, $P < 0.0001$). Yet in this model, ultrasound-based delivery of ABX (24 mg/kg) did not to significantly increase survival beyond ABX alone (41 vs. 38 days, $P = 0.3747$). However, hematoxylin and eosin (H&E) staining of untreated control mice revealed that both the MES83 and GBM12 xenografts are noninvasive and have extensive tumor vasculature, which is known to have a defective BBB (**Fig. 4E**).

ABX exhibits less neurotoxicity compared with CrEL-PTX in the setting of ultrasound-based BBB disruption

In single-course treatment toxicity tests, only mice receiving ultrasound-delivered CrEL-PTX exhibited treatment-related mortality. Two of 10 mice in the US+CrEL-PTX group died shortly after receiving intravenous CrEL-PTX injections; however, none of the surviving mice nor mice in other treatment conditions experienced any significant weight loss due to treatments (**Fig. 5A**). Twenty-one days after the single treatment, mice were sacrificed and the brains underwent histologic examination. The most common form of CNS pathology observed was vacuolation in white matter tracts of the corpus callosum. These lesions were found in 20% of mice treated with a single course of ultrasound therapy alone. No significant difference was found in CNS pathology between ultrasound therapy alone and ultrasound-based delivery of ABX at either dose tested except for one case of minor macrophage infiltration in a mouse treated with a single dose of US-ABX at 12 mg/kg. Conversely, signs of CNS pathology increased to 50% in mice that received a single dose of US-CrEL-PTX at 12 mg/kg (Supplementary Table S1).

Toxicity due to multiple courses of treatment is presented in **Table 1**. Multiple courses of ultrasound and ultrasound-delivered ABX at 12 mg/kg was generally well-tolerated and did not cause any additional signs of CNS pathology over those observed in mice receiving single-course treatments. In contrast, multiple courses of US-CrEL-PTX at an equivalent dose (12 mg/kg) produced a 58% mortality rate and caused significant necrosis and hemorrhage within the left hemisphere of the brain in 75% of the mice that died during treatment. Because CrEL has been implicated in the development of peripheral neuropathy observed in patients receiving Taxol therapy (28), we also evaluated the toxicity profile of CrEL when delivered through ultrasound. Three of 8 mice died while receiving multicourse ultrasound-delivered CrEL. One of these mice displayed similar signs of CNS pathology observed in US-CrEL-PTX–treated mice (**Fig. 5B**). When the dose of ABX delivered through ultrasound was doubled to 24 mg/kg, 5 of 25 mice experienced treatment-related toxicity. Of these 5 mice, one exhibited diffuse axonal injury, one displayed signs of cytotoxic edema, and one had focal points of white matter vacuolation. The remaining two mice displayed no signs of neurotoxicity. Interestingly, treatment-related mortality was not observed when US-ABX (24mg/kg) treatment frequency was reduced to twice a week for four weeks. Because of the significant toxicity observed with ultrasound and CrEL-PTX at 12 mg/kg, ultrasound and CrEL-PTX at 24 mg/kg was not tested.

Discussion

While the bulk of glioma tissue can often be safely resected, tumors tend to recur close to the initial presentation site, and thus, residual infiltrative tumor cells are considered to be the origin of the recurrence (36). Many systemically administered cytotoxic or molecularly targeted therapies that are effective in the treatment of other solid tumors have proven of little benefit in patients with glioma due to the
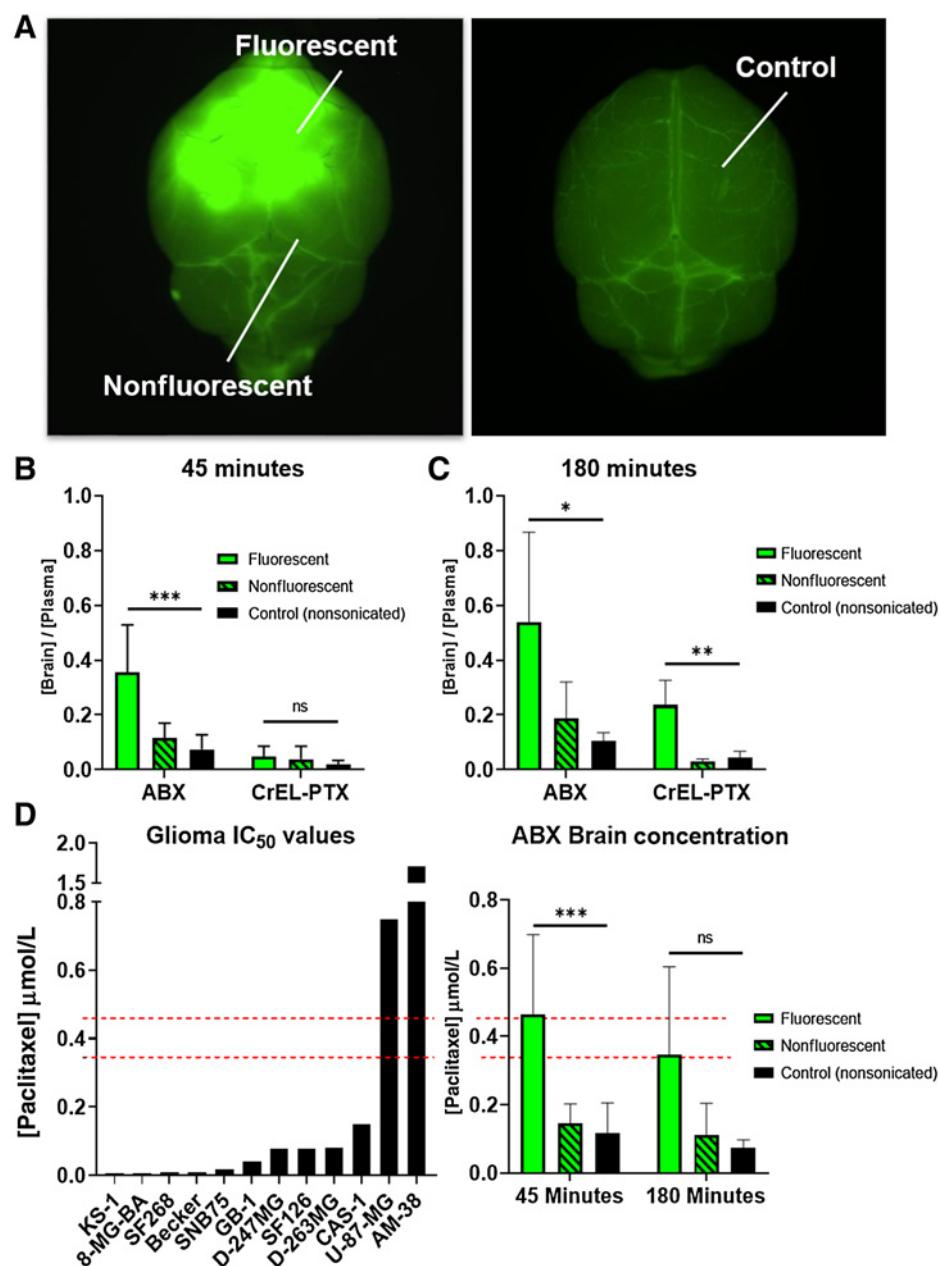
Figure 3.
Ultrasound increases ABX and CrEL-PTX brain penetration. **A,** Representative image of how samples were dissected. **B–D,** Following sonication and NaFl administration, mice were injected with either ABX or CrEL-PTX at 12 mg/kg. Paclitaxel concentration was determined in fluorescent, nonfluorescent and nonsonicated control samples through LC/MS. Data plotted are mean $\pm$ SD. Significance was determined one-way ANOVA test. Brain/plasma paclitaxel 45 minutes after sonication (***, $P = 0.0002$, ns; **B**) and brain/plasma paclitaxel 180 minutes after sonication (*, $P = 0.0241$; **, $P = 0.0017$; **C**). **D,** Absolute concentration of paclitaxel in US+ABX-treated mice compared with human glioma cell line paclitaxel IC_{50} concentration from Sanger/CCLE database (***, $P = 0.0006$, ns).

presence of the protective BBB (2). Paclitaxel displays one of the most potent antiglioma effects *in vitro*, but is unable to cross the BBB and reach infiltrative glioma cells at meaningful concentrations (27). This work demonstrates that LIPU-based disruption of the BBB may be an effective technique to enhance penetration of paclitaxel in patients with glioma.

Shen and colleagues examined the therapeutic efficacy of a liposomal paclitaxel formulation in an orthotopic GBM mouse model. Similar to our approach, they used ultrasound to open the BBB and demonstrated prolonged survival of mice suggesting meaningful antitumor activity (33). However, this study did not compare or demonstrate whether this liposomal formulation exhibits better brain penetration than other paclitaxel formulations. Moreover, there are currently no FDA-approved liposomal- -paclitaxel formulations for

use. In this study, we demonstrated the ability of ultrasound-based BBB disruption to increase paclitaxel concentrations within the brain to therapeutic levels using two FDA-approved paclitaxel formulations that are indicated for use in a variety of solid tumors such as ovarian cancer, metastatic breast cancer, metastatic pancreatic cancer, and advanced non–small cell lung cancer (19, 37). Our results show that brain penetration, distribution, efficacy, and neurotoxicity of paclitaxel is highly dependent on the vehicle solvent and chemical properties of each formulation, with ABX exhibiting improved penetration through the BBB compared with classical CrEL-PTX.

Using fluorescein, we showed that both paclitaxel formulations exhibit increased brain penetration by ultrasound-mediated opening of the BBB. However, these formulations differed in their pharmacokinetic properties following ultrasound-mediated BBB opening,
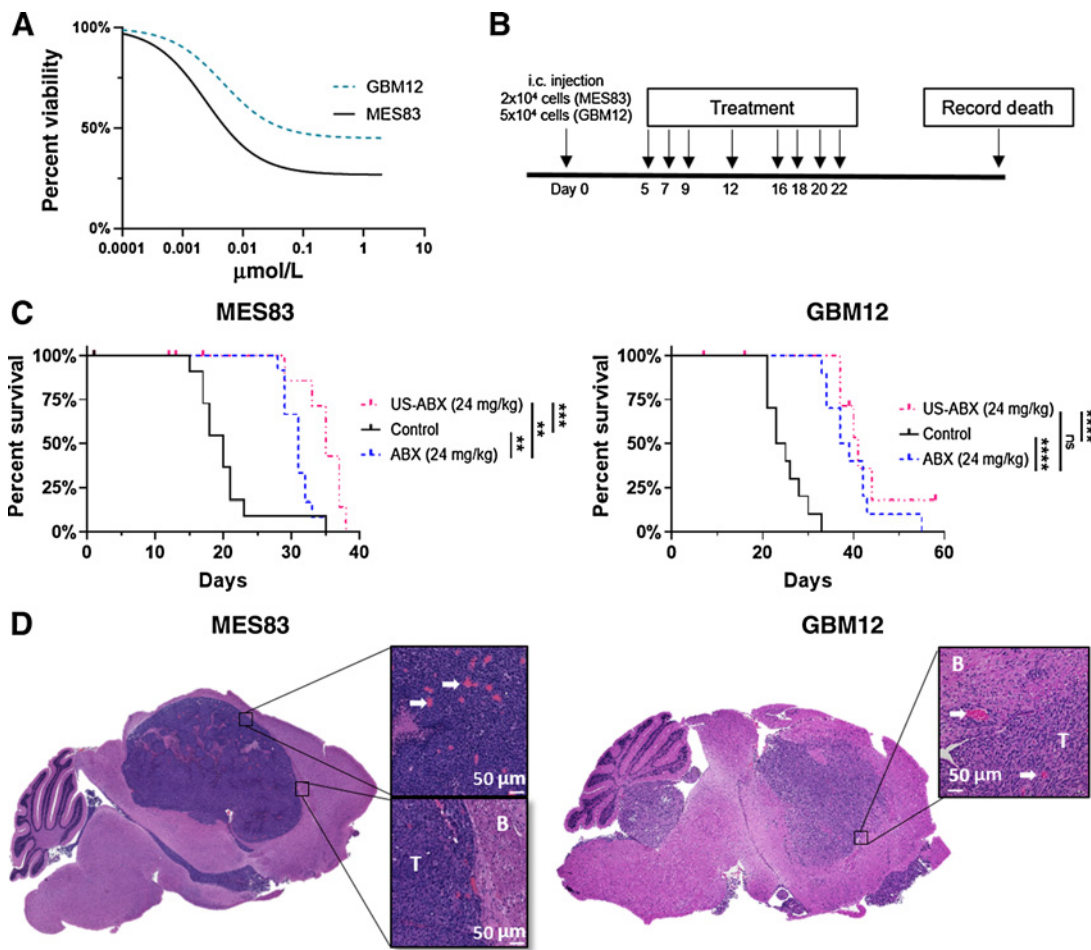
Figure 4.
Ultrasound-delivered ABX differs in therapeutic profile between two patient-derived xenograft models. **A,** Cell viability: GBM12 and MES83 short-term explant cultures were exposed to increasing doses of ABX and viability after 72 hours was determined by CellTiterGlo. Dose–response curves represent three replicates. **B,** Experimental timeline. **C,** Five days after tumor implantation, mice were randomized to treatment groups as indicated and survival is plotted through Kaplan–Meier graphs. Survival differences were determined through log-rank analysis. Mice that did not die due to tumor burden were censored from this analysis. Censored subjects are denoted by tick mark on the day they were removed from the study. (MES83: **, $P = 0.0041$; **, $P = 0.0036$; ***, $P = 0.0006$; GBM12: ****, $P < 0.0001$; ns ($P = 0.2590$); ****, $P < 0.0001$). **D,** H&E stain of tumor histology from untreated control mice. Left, MES83 xenograft. Right, GBM12 xenograft. White arrows, blood vessels. B, Brain tissue; T, Tumor mass. White scale bar, 50 µm.

specifically, ultrasound-delivered CrEL-PTX exhibited a delay in brain accumulation compared with ultrasound-delivered ABX. Forty-five minutes after BBB disruption, CrEL-PTX did not show a significant increase in B:P ratios compared with nonsonicated controls. Only at 180 minutes did ultrasound-delivered CrEL-PTX–treated mice show increased B:P ratios compared with their nonsonicated controls. In contrast, ultrasound-delivered ABX mice showed highly significant increases in paclitaxel B:P ratios at both 45 and 180 minutes. This delay in brain accumulation can, in part, be explained by the finding that CrEL forms micelles within the plasma compartment of blood, trapping paclitaxel in the circulatory system and thereby reducing its bioavailability (38).

Our toxicity studies reveal ABX is better tolerated than CrEL-PTX in the context of ultrasound-based BBB disruption. At equivalent doses (12 mg/kg), ultrasound-delivered CrEL-PTX has significantly greater rates of neurotoxicity compared with ultrasound-delivered ABX. While small patches of white matter vacuolation and macrophage

infiltration was observed in mice receiving ultrasound-delivered ABX (12 mg/kg), these lesions were indistinguishable from the lesions found in mice treated with ultrasound alone. In contrast, ultrasound-delivered CrEL-PTX induced broad swathes of necrosis and hemorrhage. Previous studies in rats have shown that CrEL plasma levels similar to those reached in the context of therapeutic CrEL-PTX dosing induce a variety of neurotoxic effects such as: axonal swelling, vesicular degeneration, and demyelination of dorsal ganglion neurons (28). Our results show that administering CrEL alone following ultrasound-mediated BBB opening is enough to induce significant neurotoxicity. These findings provide further evidence that the neurotoxic effects associated with CrEL-PTX are to a great degree, related to CrEL, the vehicle solvent of this particular formulation, rather than paclitaxel itself.

The neurotoxicity profile of the higher doses of ultrasound-delivered ABX seems to be influenced by the frequency the treatment is given. In tumor-bearing mice receiving multiple courses of
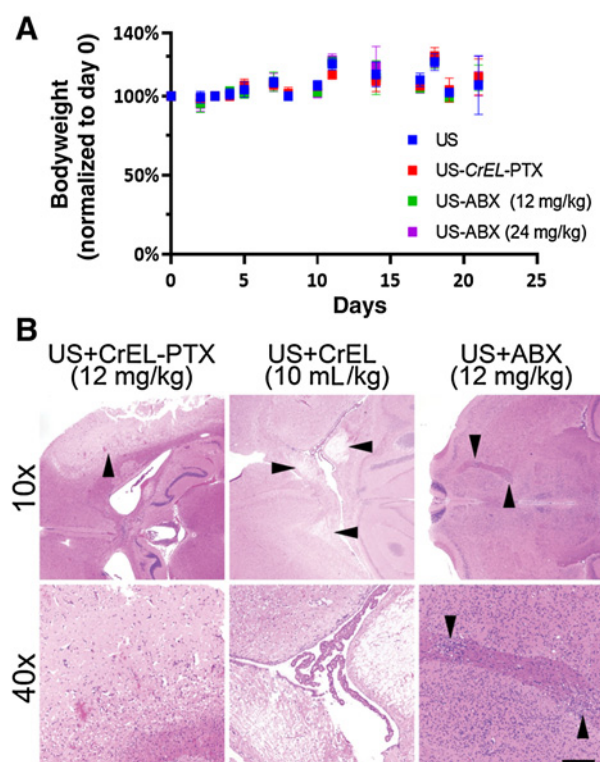
Figure 5.
Toxicity evaluation of ultrasound-delivered paclitaxel therapy. **A,** Bodyweight of mice following single course of treatment; 10 mice were evaluated for each treatment condition. Data plotted are mean ± SD. **B,** Representative photomicrographs of H&E-stained axial brain sections from mice following multiple courses of ultrasound-delivered paclitaxel. Damage was most severe in ultrasound-delivered CrEL-PTX (top left, arrowhead, and bottom left), although ultrasound-delivered CrEL alone also elicited marked white matter damage (top central, arrowheads, and bottom central). Ultrasound-delivered ABX showed only small patches of damage to deep white matter tracts in some cases (top and bottom right, arrowheads). Scale bar, 200 μm in bottom panels and 800 μm in top panels.

US-ABX at 24 mg/kg, neurotoxicity-induced death was observed in a small percentage (11.5%) of mice when the treatment was administered three times a week. Because signs of CNS pathology were observed in mice receiving multiple courses of ultrasound therapy alone, it is likely that a partial cause of the neurotoxicity observed in multicourse US-ABX mice is due to the frequency of the sonication procedure. This conclusion is further supported by the disappearance of treatment-related mortality rates when the frequency of US-ABX treatment is reduced to twice a week. Such side effects might be more likely observed in small animals, as the safety of ultrasound-mediated BBB opening in primate models and human subjects is well established, even in regimens in which sonication is performed every 3 weeks in patients with GBM (17–20).

Another interesting finding was the observation that ABX in the absence of ultrasound was able to provide a significant survival benefit despite having a similar cytotoxicity profile *in vitro* to free paclitaxel (Supplementary Fig. S2). Previous groups have hypothesized that ABX is actively transported into the tumor through endothelial glycoproteins and through the SPARC-mediated albumin binding pathway (30, 39). It is possible that the active transportation of ABX through these pathways allows for increased drug accumulation within the tumor.

We also showed that the increased paclitaxel levels within the brain parenchyma achieved by ultrasound delivery of ABX provides an increase in survival compared with ABX administration alone in one of two glioma PDX models. The observed difference in ultrasound therapeutic efficacy may be explained by the fact that GBM12 displays decreased sensitivity to ABX, with cell viability plateauing around 50% starting at 0.03 μmol/L of ABX exposure. H&E staining of GBM 12 and MES83 xenografts in untreated control mice reveal that these tumors display extensive tumor vasculature, which is known to have defective BBB, and relatively well-demarcated tumor-brain borders. It is likely that ABX is able to reach therapeutic concentrations within this tumor regardless of ultrasound-mediated delivery, masking the therapeutic benefit ultrasound may grant for infiltrative disease with intact BBB seen in patients, which cannot be easily modeled using PDX in mice.

Table 1. Toxicity evaluation from multiple courses of US-delivered chemotherapy.

| Treatment | Nontumor-bearing mice | | i.c. glioma PDX model[a] | | Total survival (%) |
	Mortality	Signs of CNS Pathology	Mortality	Signs of CNS pathology	
Ultrasound only	0/8	2/4 Small focal white matter vacuolation (WMV), Hemosiderin-laden macrophages (HLM)	0/19		27/27 (100%)
Ultrasound + Cremophor EL PTX (12 mg/kg)	4/7	3/4 severe necrosis, hemorrhage, Diffuse axonal injury (DAI), hippocampal damage			3/7 (42%)
Ultrasound + Cremophor EL (5% in Saline)	3/8	1/3 DAI 2/3 small focal WMV			5/8 (62.5%)
Ultrasound + Abraxane (12 mg/kg)	1/6	3/4 Focal WMV	0/20		25/26 (96%)
Ultrasound + Abraxane (24 mg/kg)	0/5	1/3 HLM	5/21	1/3 cytotoxic edema 1/3 DAI 1/3 focal WMV	21/26 (81%)
Ultrasound + Abraxane[b] (24 mg/kg)			0/10		10/10 (100%)

[a]In intracranial glioma PDX model mice, deaths were considered due to treatment if the day of death was considered significantly different from control untreated tumor-bearing mice ($P < 0.0005$).
[b]Mice received treatment twice a week (MTh) × 4 weeks instead of 8 courses of treatment over 3 weeks.

Early attempts to disrupt the BBB through ultrasound were thwarted by the inability for ultrasound waves to bypass the human skull. Two methods have been developed to overcome this obstacle. The first, transcranial focused ultrasound (FUS), uses a large external ultrasound transducer that is either single or multi-element to generate a focused ultrasound beam to target a specific focal region of the brain for BBB disruption. Guidance of the treatment is then performed using either neuronavigation or MR guidance, with ultrasound feedback to control the sonication output parameters (18). The second method is an ultrasound device directly implanted into a cranial window on the patient's skull. While both methods of US-BBB disruption are well tolerated, they have their own associated advantages and limitations (18, 20). Transcranial FUS allows for more precise targeting of BBB disruption; however, the relatively small region of BBB disruption may not be sufficient to cover the areas where residual tumor cells may be residing following tumor resection. On the other hand, the most recent iteration of the implantable ultrasound device developed by Carthera, Sonocloud-9, features nine ultrasound transducer heads that are designed to sonicate the tumor and surrounding infiltrative region (40).

As ultrasound-mediated BBB disruption for drug delivery moves from preclinical to clinical studies, the ability to quantify the concentration of the therapeutic agent delivered into the brain parenchyma via ultrasound-mediated BBB opening may be of importance (40). Currently, BBB disruption by ultrasound is validated by the use of Evan's Blue injection in animal models or by MRI gadolinium contrast enhancement in patients (19, 41). One drawback to MRI visualization of BBB opening is this method does not allow for real-time tissue sampling of regions of ultrasound BBB disruption. On an initial pharmacokinetic human study of the effect of ultrasound on drug concentrations, tissue for analysis was collected one day after MRI confirmation of ultrasound-mediated BBB opening (18). This delay and inaccuracy in sampling of tissue subject to BBB disruption can negatively impact the measurement of therapeutic agent concentration achieved by ultrasound delivery in humans. Because NaFl has been established as an intraoperative tool to guide glioma resection (42), we sought to investigate its ability as a visual marker for ultrasound-based BBB. Our study establishes the ability of NaFl to map BBB disruption following a 45-minute incubation period, which is feasible in the operating room. Thus, we believe that in future clinical trials, NaFl can be repurposed to guide sampling of peritumoral brain tissue subject to ultrasound-based BBB disruption in real-time. This would allow for intraoperative pharmacokinetic studies to directly investigate the effect of ultrasound-based BBB disruption on the concentration of chemotherapeutics in the peritumoral brain.

Other interesting formulations of paclitaxel designed to bypass the BBB are in early preclinical and clinical development. In particular, GRN-1005, a novel paclitaxel–peptide conjugate has been explored in the context of gliomas and brain metastases (43). GRN-1005 relies on low-density lipoprotein receptor-related protein-1 (LRP-1)-mediated transcytosis to deliver paclitaxel across the BBB. A recent phase I clinical trial investigating GRN-1005 in patients with recurrent glioma reported paclitaxel levels in excised tumor tissue generally exceeded plasma levels in patients treated with GRN-1005. Furthermore, patients exhibited no signs of CNS toxicity even when GRN-1005 was administered at 650 mg/m^2 (44). A phase II study aimed at evaluating efficacy of this drug in the treatment of GBM was recently completed in 2017, the results of which are eagerly awaited.

In conclusion, novel methods for the treatment of GBM are urgently needed. Paclitaxel displays high cytotoxicity against glioma, yet this efficacy has not been exploited due to the protective BBB. In this study, we have demonstrated the feasibility, safety, and efficacy of repeated ultrasound delivery of ABX. Ultrasound is a well tolerated and effective way to increase drug delivery to the human brain and ABX is a well-characterized FDA-approved formulation of paclitaxel. In this context, systemic administration of ABX with concomitant ultrasound-based BBB disruption with LIPU is a novel treatment of high therapeutic value that is well positioned to be explored in clinical trials.

Authors' Contributions

Conception and design: D.Y. Zhang, C.D. James, A. Carpentier, M. Canney, R. Stupp, A.M. Sonabend

Development of methodology: D.Y. Zhang, V.A. Arrieta, L.P. Magnusson, A. Baran, C.D. James, A. Carpentier, M. Canney, M. Muzzio, R. Stupp, A.M. Sonabend

Acquisition of data (provided animals, acquired and managed patients, provided facilities, etc.): D.Y. Zhang, C. Dmello, V.A. Arrieta, E. Gonzalez-Buendia, L.P. Magnusson, C. Horbinski, A. Carpentier, M. Muzzio, R. Stupp, A.M. Sonabend, J.R. Kane

Analysis and interpretation of data (e.g., statistical analysis, biostatistics, computational analysis): D.Y. Zhang, C. Dmello, V.A. Arrieta, C. Horbinski, R. Stupp, A.M. Sonabend, J.R. Kane

Writing, review, and/or revision of the manuscript: D.Y. Zhang, C.D. James, C. Desseaux, M. Canney, A.M. Sonabend

Administrative, technical, or material support (i.e., reporting or organizing data, constructing databases): L. Chen, C.D. James, M. Canney

Study supervision: A.M. Sonabend

References

1. Stupp R, Taillibert S, Kanner A, Read W, Steinberg D, Lhermitte B, et al. Effect of tumor-treating fields plus maintenance temozolomide vs maintenance temozolomide alone on survival in patients with glioblastoma: a randomized clinical trial. JAMA 2017;318:2306–16.
2. Pitz MW, Desai A, Grossman SA, Blakeley JO. Tissue concentration of systemically administered antineoplastic agents in human brain tumors. J Neuro-Oncol 2011;104:629–38.
3. Pardridge WM. The blood-brain barrier: bottleneck in brain drug development. NeuroRx 2005;2:3–14.
4. Long DM. Capillary ultrastructure and the blood-brain barrier in human malignant brain tumors. J Neurosurg 1970;32:127–44.
5. Kane JR. The role of brain vasculature in glioblastoma. Mol Neurobiol 2019;56: 6645–53.
6. van Tellingen O, Yetkin-Arik B, de Gooijer MC, Wesseling P, Wurdinger T, de Vries HE. Overcoming the blood-brain tumor barrier for effective glioblastoma treatment. Drug Resist Updat 2015;19:1–12.
7. Bobo RH, Laske DW, Akbasak A, Morrison PF, Dedrick RL, Oldfield EH. Convection-enhanced delivery of macromolecules in the brain. Proc Natl Acad Sci U S A 1994;91:2076–80.
8. Allhenn D, Boushehri MA, Lamprecht A. Drug delivery strategies for the treatment of malignant gliomas. Int J Pharm 2012;436:299–310.
9. Jahangiri A, Chin AT, Flanigan PM, Chen R, Bankiewicz K, Aghi MK. Convection-enhanced delivery in glioblastoma: a review of preclinical and clinical studies. J Neurosurg 2017;126:191–200.
10. Kunwar S, Chang S, Westphal M, Vogelbaum M, Sampson J, Barnett G, et al. Phase III randomized trial of CED of IL13-PE38QQR vs Gliadel wafers for recurrent glioblastoma. Neuro Oncol 2010;12:871–81.
11. Zunkeler B, Carson RE, Olson J, Blasberg RG, DeVroom H, Lutz RJ, et al. Quantification and pharmacokinetics of blood-brain barrier disruption in humans. J Neurosurg 1996;85:1056–65.
12. Choi JJ, Pernot M, Small SA, Konofagou EE. Noninvasive, transcranial and localized opening of the blood-brain barrier using focused ultrasound in mice. Ultrasound Med Biol 2007;33:95–104.
13. Aryal M, Park J, Vykhodtseva N, Zhang YZ, McDannold N. Enhancement in blood-tumor barrier permeability and delivery of liposomal doxorubicin using focused ultrasound and microbubbles: evaluation during tumor progression in a rat glioma model. Phys Med Biol 2015;60:2511–27.
14. Drean A, Lemaire N, Bouchoux G, Goldwirt L, Canney M, Goli L, et al. Temporary blood-brain barrier disruption by low intensity pulsed ultrasound increases carboplatin delivery and efficacy in preclinical models of glioblastoma. J Neurooncol 2019;144:33–41.
15. Beccaria K, Canney M, Goldwirt L, Fernandez C, Piquet J, Perier MC, et al. Ultrasound-induced opening of the blood-brain barrier to enhance temozolomide and irinotecan delivery: an experimental study in rabbits. J Neurosurg 2016; 124:1602–10.
16. Kovacs ZI, Tu TW, Sundby M, Qureshi F, Lewis BK, Jikaria N, et al. MRI and histological evaluation of pulsed focused ultrasound and microbubbles treatment effects in the brain. Theranostics 2018;8:4837–55.
17. Wu SY, Aurup C, Sanchez CS, Grondin J, Zheng W, Kamimura H, et al. Efficient blood-brain barrier opening in primates with neuronavigation-guided ultrasound and real-time acoustic mapping. Sci Rep 2018;8:7978.
18. Mainprize T, Lipsman N, Huang Y, Meng Y, Bethune A, Ironside S, et al. Blood-brain barrier opening in primary brain tumors with non-invasive MR-guided focused ultrasound: a clinical safety and feasibility study. Sci Rep 2019;9:321.
19. Carpentier A, Canney M, Vignot A, Reina V, Beccaria K, Horodyckid C, et al. Clinical trial of blood-brain barrier disruption by pulsed ultrasound. Sci Transl Med 2016;8:343re2.
20. Idbaih A, Canney M, Belin L, Desseaux C, Vignot A, Bouchoux G, et al. Safety and feasibility of repeated and transient blood-brain barrier disruption by pulsed ultrasound in patients with recurrent glioblastoma. Clin Cancer Res 2019;25: 3793–801.
21. Barretina J, Caponigro G, Stransky N, Venkatesan K, Margolin AA, Kim S, et al. The Cancer Cell Line Encyclopedia enables predictive modelling of anticancer drug sensitivity. Nature 2012;483:603–7.
22. Chamberlain MC, Kormanik P. Salvage chemotherapy with paclitaxel for recurrent primary brain tumors. J Clin Oncol 1995;13:2066–71.
23. Prados MD, Schold SC, Spence AM, Berger MS, McAllister LD, Mehta MP, et al. Phase II study of paclitaxel in patients with recurrent malignant glioma. J Clin Oncol 1996;14:2316–21.
24. Fetell MR, Grossman SA, Fisher JD, Erlanger B, Rowinsky E, Stockel J, et al. Preirradiation paclitaxel in glioblastoma multiforme: efficacy, pharmacology, and drug interactions. New Approaches to Brain Tumor Therapy Central Nervous System Consortium. J Clin Oncol 1997;15:3121–8.
25. Chang SM, Kuhn JG, Rizzo J, Robins HI, Schold SC Jr, Spence AM, et al. Phase I study of paclitaxel in patients with recurrent malignant glioma: a North American Brain Tumor Consortium report. J Clin Oncol 1998;16:2188–94.
26. Heimans JJ, Vermorken JB, Wolbers JG, Eeltink CM, Meijer OW, Taphoorn MJ, et al. Paclitaxel (Taxol) concentrations in brain tumor tissue. Ann Oncol 1994;5: 951–3.
27. Heimans JJ, Taphoorn MJ, Vermorken JB, Eeltink C, Wolbers JG, Meijer OW, et al. Does paclitaxel penetrate into brain tumor tissue? J Natl Cancer Inst 1995; 87:1804–5.
28. Authier N, Gillet JP, Fialip J, Eschalier A, Coudore F. Assessment of neurotoxicity following repeated cremophor/ethanol injections in rats. Neurotox Res 2001;3: 301–6.
29. Windebank AJ, Blexrud MD, de Groen PC. Potential neurotoxicity of the solvent vehicle for cyclosporine. J Pharmacol Exp Ther 1994;268:1051–6.
30. Gradishar WJ. Albumin-bound paclitaxel: a next-generation taxane. Expert Opin Pharmacother 2006;7:1041–53.
31. Gradishar WJ, Tjulandin S, Davidson N, Shaw H, Desai N, Bhar P, et al. Phase III trial of nanoparticle albumin-bound paclitaxel compared with polyethylated castor oil–based paclitaxel in women with breast cancer. J Clin Oncol 2005;23: 7794–803.
32. Carlson BL, Pokorny JL, Schroeder MA, Sarkaria JN. Establishment, maintenance and in vitro and in vivo applications of primary human glioblastoma multiforme (GBM) xenograft models for translational biology studies and drug discovery. Curr Protoc Pharmacol 2011;Chapter 14:Unit 14.16.
33. Shen Y, Pi Z, Yan F, Yeh CK, Zeng X, Diao X, et al. Enhanced delivery of paclitaxel liposomes using focused ultrasound with microbubbles for treating nude mice bearing intracranial glioblastoma xenografts. Int J Nanomedicine 2017;12:5613–29.
34. Hodgson JG, Yeh RF, Ray A, Wang NJ, Smirnov I, Yu M, et al. Comparative analyses of gene copy number and mRNA expression in glioblastoma multiforme tumors and xenografts. Neuro Oncol 2009;11:477–87.
35. Mao P, Joshi K, Li J, Kim SH, Li P, Santana-Santos L, et al. Mesenchymal glioma stem cells are maintained by activated glycolytic metabolism involving aldehyde dehydrogenase 1A3. Proc Natl Acad Sci U S A 2013;110:8644–9.
36. Hochberg FH, Pruitt A. Assumptions in the radiotherapy of glioblastoma. Neurology 1980;30:907–11.
37. Skog J, Würdinger T, van Rijn S, Meijer DH, Gainche L, Sena-Esteves M, et al. Glioblastoma microvesicles transport RNA and proteins that promote tumour growth and provide diagnostic biomarkers. Nat Cell Biol 2008;10: 1470–6.
38. Sparreboom A, van Zuylen L, Brouwer E, Loos WJ, de Bruijn P, Gelderblom H, et al. Cremophor EL-mediated alteration of paclitaxel distribution in human blood. Clin Pharm Impl 1999;59:1454–7.
39. Trieu V, Frankel T, Labao E, Soon-Shiong P, Desai N. SPARC expression in breast tumors may correlate to increased tumor distribution of nanoparticle albumin-bound paclitaxel (ABI-007) vs taxol. Cancer Res 2005;65:1314.
40. Sonabend AM, Stupp R. Overcoming the blood-brain barrier with an implantable ultrasound device. Clin Cancer Res 2019;25:3750–2.
41. Yang FY, Lee PY. Efficiency of drug delivery enhanced by acoustic pressure during blood-brain barrier disruption induced by focused ultrasound. Int J Nanomedicine 2012;7:2573–82.
42. Shinoda J, Yano H, Yoshimura S, Okumura A, Kaku Y, Iwama T, et al. Fluorescence-guided resection of glioblastoma multiforme by using high-dose fluorescein sodium. Technical note. J Neurosurg 2003;99:597–603.
43. Regina A, Demeule M, Ché C, Lavallée I, Poirier J, Gabathuler R, et al. Antitumour activity of ANG1005, a conjugate between paclitaxel and the new brain delivery vector Angiopep-2. Br J Pharmacol 2008;155:185–97.
44. Drappatz J, Brenner A, Wong ET, Eichler A, Schiff D, Groves MD, et al. Phase I study of GRN1005 in recurrent malignant glioma. Clin Cancer Res 2013;19:1567–76.